Anomalous Rheological Behavior of Ordered Phases of Block Copolymers. 2

Masao Doi,*,† James L. Harden,† and Takao Ohta‡

Department of Applied Physics, Nagoya University, Chikusa-ku, Nagoya 464, Japan, and Department of Physics, Faculty of Science, Ochanomizu University, Bunkyo-ku, Tokyo 112, Japan

Received March 5, 1993; Revised Manuscript Received June 7, 1993

ABSTRACT: We present a statistical theory for the rheology of the ordered, mesophase state of block copolymers based on a coupled multilayer model. We apply this model to the cases of steady shear flow, stress relaxation after a step-strain, and applied oscillatory shear strains. This theory predicts various novel nonlinear rheological responses associated with the relative slippage of macrolattice planes. In particular, we find (i) viscoplastic flow behavior with a true yield stress, (ii) a novel double stress relaxation in response to sufficiently large applied step-strains, and (iii) unusual nonlinear stress–strain patterns in response to applied oscillatory shear strains of sufficient amplitude, including lozenge-shaped stress–strain patterns at very low frequencies and strain-hardened patterns at high frequencies. Our theory qualitatively reproduces the oscillatory and step-strain rheological behavior found in the simulation of cylindrical mesophases of block copolymer under applied shear.[1] We discuss the possible relevance of our model to experimental rheological and structural studies of microphase-separated block copolymer solutions in selective solvents and to more general cases of ordered liquids.

1. Introduction

When block copolymers form ordered phases by microphase separation, their rheological properties change drastically. In the disordered state, the rheological responses are those of typical viscoelastic liquids. There is a clear regime of linear viscoelasticity: the viscosity approaches a constant value at low shear rate, and the storage modulus $G'(\omega)$ and the loss modulus $G''(\omega)$ behave as $G'(\omega) \sim \omega$ and $G''(\omega) \sim \omega^2$ at low frequency. This low frequency scaling of G' and G'' with ω holds even near the order–disorder transition temperature, although it is accompanied by a strong increase in the magnitude of the low frequency moduli associated with large scale composition fluctuations near the microphase transition point.[2,3]

When an ordered phase is formed, however, the rheological behavior becomes quite unusual and often strongly nonlinear. The steady state viscosity increases indefinitely as the shear rate is lowered (yield behavior). Furthermore, the complex modulus does not exhibit the typical terminal frequency dependence at low frequencies. In the lamellar phase, for instance, the storage and loss moduli have the same anomalous low frequency scaling behavior:[2,4,5] $G'(\omega) \sim G''(\omega) \sim \omega^\alpha$ with $\alpha \simeq 0.5$. The domain structure of these ordered mesophases is responsible for this complex rheological behavior, in part because dynamic processes must occur on both microscopic and mesoscopic length scales in these systems. On microscopic scales, the rheology is affected by the release of interdomain chain entanglements, while on mesoscopic scales, collective dynamic processes such as domain deformation and relative displacement of domains are relevant. Topological defects present in imperfectly ordered mesophases also affect rheological properties.[6]

Theoretical studies of the rheology of microphase-separated block copolymers have been restricted, for the most part, to the linear viscoelasticity of the lamellar mesophase. The viscoelasticity of the lamellar phase was first discussed in terms of the nature of interdomain chain entanglements and their relaxation behavior in response to applied stress by Witten, Leibler, and Pincus.[7] This approach was extended and refined by Rubinstein and Obukhov[8] to include the effect of fluctuations in the number of interdomain entanglements on stress relaxation and has also been adopted to discuss the viscous friction between molten polymer brushes in shedar flow,[9] a situation perhaps analogous to the lamellar phase in shear flow. The effects of domain collective dynamics on the low frequency rheology of the lamellar phase was studied by Kawasaki and Onuki.[10] They demonstrated that overdamped second-sound modes in an orientationally disordered lamellar phase could result in anomalous low frequency rheological behavior with $G'(\omega) \sim G''(\omega) \sim \omega^{1/2}$, consistent with experimental findings.[2,4,5] Rubinstein and Obukhov also obtained this result through the consideration of diffusion-controlled annihilation of defects in disordered lamellar systems.[8]

None of the above studies, however, considers the rheological behavior due to relative displacement of domains in an ordered mesophase. Such collective dynamics may be especially important in spherical or cylindrical mesophases, which form two- or three-dimensional ordered macrolattices. In these systems, strong nonlinear rheological effects associated with spatially periodic interdomain potentials are anticipated.

Recently, computer simulation of the rheology of the ordered cylindrical mesophase of block copolymers was carried out by Ohta *et al.*[1] Their results indicated some very anomalous rheological responses in the ordered phase, such as the following: (1) When an oscillatory shear strain of sufficient magnitude is applied, the Lissajous pattern (the plot of stress against strain) is elliptic at high frequency but resembles a parallelogram or lozenge at low frequency. This lozenge pattern is not observed for low amplitude shear strains. (2) When a sufficiently large step-strain is applied, the stress first relaxes rapidly to a pseudosteady value, and then relaxes once again to a smaller value after a considerable delay. Ohta *et al.*[1] showed that such anomalous relaxation takes place when the relative slippage of macrolattice planes occurs.

In this paper, we shall study the phenomena of lattice plane slippage using a simple model. We consider a multilayer system of macrolattice planes which interact

* To whom correspondence should be addressed.
† Nagoya University.
‡ Ochanomizu University.

0024-9297/93/2226-4935$04.00/0 © 1993 American Chemical Society

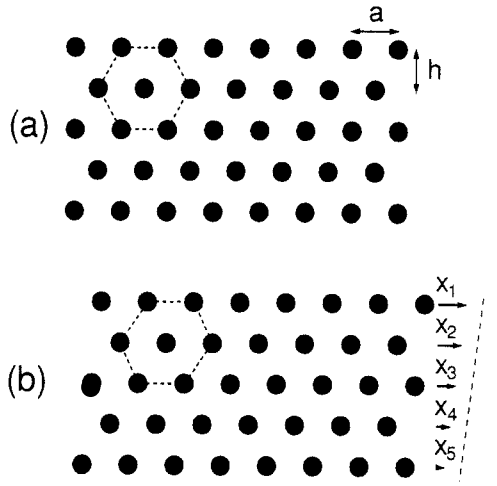

Figure 1. Sketch of a cross section of a cylindrical mesophase in the equilibrium and deformed states. In (a), the equilibrium hexagonal macrolattice with lattice constant a and interlayer separation h is shown. In (b), each lattice plane is displaced a distance x_i due to a shear strain applied in the horizontal direction. The dashed lines in (a) and (b) indicate, respectively, the equilibrium and sheared hexagonal unit cells.

with each other via periodic potential and calculate the system response when the top layer is sheared relative to the bottom. We will show that this simple model explains the characteristic features of the rheology of the ordered phases in the simulations and also qualitatively reproduces some of the rheological behavior observed in experiments on microphase-separated block copolymer solutions in selective solvents.[11-13]

In section 2, we describe the features of our model and give an explicit expression for the macroscopic stress–strain constitutive relation in terms of interlayer stresses and strains. We argue that the deformation of such a system is typically characterized by many different modes of interlayer displacement corresponding to the relative slippage of lattice planes, and we demonstrate the essential role of fluctuations or disorder in selection of such a slipping mode. In section 3, we develop a statistical theory of deformation based on the model presented in section 2 which accounts for the role of intrinsic disorder in a natural way. In section 4, we apply this statistical approach, augmented by numerical calculations, to the specific cases of steady shear flow, stress relaxation after an applied step-strain, and applied oscillatory shear strain. In section 5, we summarize and discuss our approach and findings. We compare our results to those obtained in the numerical simulations presented in the previous paper[1] and to experimental studies of the rheology of microphase-separated block copolymer solutions.[11-13] We also discuss the possible relevance of our model to the rheology of mesophases of homopolymer/copolymer mixtures and other ordered fluids. Finally, we discuss possible directions for future theoretical study.

2. Model

We consider a two-dimensional array of microphase-separated diblock copolymer domains, as shown in Figure 1. In equilibrium, the domains form a regular hexagonal lattice (Figure 1a). Such a situation is an idealized representation of a cross section of the cylindrical mesophase. When shear strain is applied, however, the domains are displaced relative to each other and also their shapes are changed. A complete description of such a process is complicated and beyond the scope of this paper. Instead, we use a simple model that focusses on the interlayer domain displacement.

In this model, the shear deformation is characterized by the horizontal displacement x_i of each layer (Figure 1b). The deformation and subsequent relaxation of the domains is not taken into account explicitly but is accounted for implicitly through the addition of viscoelastic terms. Note that domain displacements within each layer are not considered. Thus, the state of the system is entirely characterized by the following dimensionless parameters

$$\gamma_i = 2\pi\frac{x_{i+1} - x_i}{a} \tag{2.1}$$

where a is the periodicity of the lattice structure and i is the layer index (see Figure 1). Notice that γ_i is related to the local shear strain $\tilde{\gamma}_i \equiv (x_{i+1} - x_i)/h$, h being the distance between the layers, by

$$\gamma_i = 2\pi\frac{h}{a}\tilde{\gamma}_i \tag{2.2}$$

Since γ_i and $\tilde{\gamma}_i$ are strictly proportional, we shall refer to γ_i simply as the shear strain in the following and make the conversion to real shear strains when necessary.

We now consider the shear stress σ_i acting between the $i+1$ and ith layers. In equilibrium, $\sigma_i(t)$ must be a periodic function of $\gamma_i(t)$

$$\sigma_i(t) = F(\gamma_i(t)) \quad \text{with} \quad F(\gamma_i + 2\pi) = F(\gamma_i) \tag{2.3}$$

However, if the system is not in equilibrium, viscoelastic effects are important. Therefore, a natural model for the relation between stress and strain for each layer of block copolymer domains is

$$\sigma_i(t) = F(\gamma_i(t)) + \int_{-\infty}^{t} dt'\, G(t-t')\dot{\gamma}_i(t') \tag{2.4}$$

where $G(t)$ is a relaxation function which vanishes asymptotically as $t \to \infty$.

To explicitly carry out the analysis, we must specify $F(\gamma)$ and $G(t)$. The elastic term $F(\gamma)$ can be obtained theoretically. Watanabe and Kotaka[14] calculated the linear elastic modulus of model spherical mesophases using the mean field theory of Helfand.[15] $F(\gamma)$ can be obtained by extending such a calculation into the nonlinear regime. However, the essential physics may be obtained if we assume the following simple form

$$F(\gamma) = G_1 \sin\gamma \tag{2.5}$$

The relaxation modulus $G(t)$ has perhaps two origins. One is the deformation of individual chains. This is the dominant mechanism for the viscoelasticity in the disordered state and should be important in the ordered state as well.[7,8] The other contribution to $G(t)$ is the deformation of the domains. When the system is sheared, the domains are first deformed affinely but then relax to their equilibrium shape with a finite relaxation time. Therefore, $G(t)$ should be characterized by at least two relaxation times. The former processes generally occur much more rapidly than the latter. Hence we assume, again for the sake of simplicity, a single relaxation time, *i.e.* the following form:

$$G(t) = G_2 \exp(-t/\tau) \tag{2.6}$$

where G_2 and τ are the characteristic transient modulus and relaxation time corresponding to domain deformation. Note that the domain relaxation time τ is much larger that the characterisetic relaxation time of interdomain chain entanglements. Hence, our theory will focus on very slow structural relaxation processes. Equations 2.4–2.6 describe the local stress–strain relation for each layer.

The macroscopic stress–strain relation for the multilayer system can be obtained easily from these equations. Under usual conditions inertial effects are negligible, implying that the shear stress is uniform throughout the material, *i.e.* all σ_i must be equal. We thus replace σ_i by the macroscopic shear stress σ, to obtain

$$\sigma(t) = G_1 \sin(\gamma_i(t)) + \int_{-\infty}^{t} dt'\, G_2 \exp(-(t-t')/\tau)\dot{\gamma}_i(t') \quad (2.7)$$

The macroscopic strain $\bar{\gamma}$ is simply the average of the local layer strains:

$$\bar{\gamma} = \frac{1}{N}\sum_{i=1}^{N} \gamma_i \quad (2.8)$$

where N is the number of layers in the system. Equations 2.7 and 2.8 define the relation between the macroscopic stress σ and macroscopic strain $\bar{\gamma}$.

In the following, we shall develop equations in a dimensionless form. We choose G_1 as the unit of stress (or elastic constant) and τ as the unit of time. Thus eq 2.7 is written as

$$\sigma(t) = \sin(\gamma_i(t)) + \int_{-\infty}^{t} dt'\, G \exp[-(t-t')]\dot{\gamma}_i(t') \quad (2.9)$$

where $G = G_2/G_1$. Equation 2.9 can also be expressed in a differential form:

$$(G + \cos\gamma_i)\dot{\gamma}_i + \sin\gamma_i = \sigma + \dot{\sigma} \quad (2.10)$$

The latter form is convenient for studying layer slippage.

Rheological experiments are done either by controlling the strain and measuring the stress (strain-controlled case) or by controlling the stress and measuring the strain (stress-controlled case). Strain-controlled experiments are most common, but stress-controlled experiments can be done as well. Both cases can be discussed within the framework of the present model.

(A) Strain-Controlled Case. Here $\bar{\gamma}(t)$ is a given function of time and $\gamma_i(t)$ and $\sigma(t)$ are to be determined from eqs 2.8 and 2.10. A trivial solution is $\gamma_i(t) = \bar{\gamma}(t)$ for all i, which we shall refer to as the homogeneous solution. If this were the only solution, no further analysis would be needed. However, under some conditions, the homogeneous solution becomes unstable, and many other solutions appear. This can be demonstrated by a simple example.

Consider a step-strain experiment. Suppose a step-strain $\bar{\gamma}$ is applied at time $t = 0$. If all γ_i are strictly equal to $\bar{\gamma}$ at $t = 0_+$, then they remain so for $t > 0$. In practice, however, there are some fluctuations. Let us consider how the fluctuations $\delta\gamma_i = \gamma_i(t) - \bar{\gamma}$ propagate in time. Linearizing eqs 2.8 and 2.10 with respect to $\delta\gamma_i$ and $\delta\sigma = \sigma - \bar{\sigma}$, we have

$$\sum_{i=1}^{N} \delta\gamma_i = 0 \quad (2.11)$$

$$(G + \cos\bar{\gamma})\delta\dot{\gamma}_i + \cos(\bar{\gamma})\delta\gamma_i = \delta\sigma + \delta\dot{\sigma} \quad (2.12)$$

From eq 2.11, it follows that the right hand side of eq 2.12 is equal to zero, and hence

$$\delta\dot{\gamma}_i = -\frac{\cos\bar{\gamma}}{G + \cos\bar{\gamma}}\delta\gamma_i \quad (2.13)$$

If $\bar{\gamma} > \pi/2$, the coefficient of $\delta\gamma_i$ on the right hand side of eq 2.13 is positive. Therefore, the fluctuation grows exponentially in time, and a bifurcation of the solution takes place. This is the origin of the anomalous stress relaxation observed in the computer simulations, as we shall show later.

(B) Stress-Controlled Case. In the stress-controlled case, the analysis of the equations becomes very simple since the equations for γ_i are uncoupled; eq 2.10 can be solved for each γ_i, and then the total strain is calculated by eq 2.8. However, even in this case, the solution is not trivial because bifurcations also take place when the stress becomes large.

3. Probability Distribution Function

3.1. Necessity of the Noise Term. As we have shown, the time evolution equation for γ_i has multiple solutions. Apart from the homogeneous solution, these solutions correspond to layer slippage. Our aim here is to study the statistics of such slippage. In such a problem, it is important to introduce some randomness because, as we have indicated in the previous section, the statistics of the slippage depends sensitively on small fluctuations in γ_i. Here we shall assume (rather arbitrarily) that each γ_i is subject to a stationary noise source. Thus, instead of eq 2.10, γ_i satisfies

$$\dot{\gamma}_i = \frac{\sigma + \dot{\sigma} - \sin(\gamma_i)}{G + \cos(\gamma_i)} + f_i(t) \quad (3.1)$$

where $f_i(t)$ is a Gaussian white noise satisfying $\langle f_i(t)\rangle = 0$ and $\langle f_i(t) f_j(t')\rangle = 2D\delta_{ij}\delta(t-t')$. Here D is a constant (having the dimension of time^{-1}) which characterizes the strength of the noise.

Although eq 3.1 may appear a natural model for a many layer system, interpretation of the noise term $f_i(t)$ is a rather subtle issue. A naive interpretation is that $f_i(t)$ simply represents thermal fluctuations. However, since γ_i (or x_i) represents the average displacement of many domains belonging to a given lattice plane, the fluctuations of γ_i should not be large. Indeed, the thermal fluctuations $\langle\delta\gamma_i^2\rangle$ should decrease as the number of domains belonging to a lattice plane N_d increases, *i.e.* $\langle\delta\gamma_i^2\rangle \propto 1/N_d$. Hence it is not realistic to assume that f_i arises from thermal fluctuations. A more realistic interpretation is that f_i represents the effects of some structural imperfections, *e.g.* imperfect ordering of domains, polydispersity of domain sizes, etc. From this point of view, the noise term is the result of integrating out the internal degrees of freedom within the weakly disordered layers. Whether one can represent the effects of structural disorder by a white noise term is not clear. At this stage, we use the noise term because it is a well defined model for disorder that has been studied in detail.[16] We expect, however, that the use of more realistic models of disorder will only result in quantitative differences in the rheological properties.

3.2. Diffusion Equation. To consider the statistics of slippage, we consider the probability $P(\gamma,t)d\gamma$ of finding a layer with shear strain between γ and $\gamma + d\gamma$. It is important to note that, due to the periodicity of the system, the shear strain γ and $\gamma + 2\pi$ correspond to the same physical state. Therefore we may assume that $P(\gamma,t)$ is a periodic function of γ:

$$P(\gamma + 2\pi, t) = P(\gamma, t) \quad (3.2)$$

Furthermore, we impose the following normalization condition for $P(\gamma,t)$:

$$\int_0^{2\pi} P(\gamma,t)\, d\gamma = 1 \quad (3.3)$$

The time evolution equation for $P(\gamma,t)$ can be obtained by

the standard procedure.[16] For the sake of simplicity, we assume $G \gg 1$ and write eq 3.1 as

$$\dot{\gamma}_i = -\frac{\partial U}{\partial \gamma_i} + f_i(t) \tag{3.4}$$

with

$$U(\gamma,t) = -[(\sigma + \dot{\sigma})\gamma + \cos\gamma]/G \tag{3.5}$$

Then, $P(\gamma,t)$ satisfies

$$\frac{\partial P}{\partial t} = D\frac{\partial^2 P}{\partial \gamma^2} + \frac{\partial}{\partial \gamma}\left(\frac{\partial U}{\partial \gamma}P\right) \tag{3.6}$$

It should be noted that the average shear strain $\bar{\gamma}$ cannot be calculated directly from $P(\gamma,t)$, since we have imposed the periodicity of $P(\gamma,t)$. However, the average shear rate $\dot{\bar{\gamma}}$ can be calculated by taking the average of the net flux:

$$\dot{\bar{\gamma}} = \int_0^{2\pi}\left(-D\frac{\partial P}{\partial \gamma} - \frac{\partial U}{\partial \gamma}P\right) d\gamma \tag{3.7}$$

The integral of the first term vanishes due to eq 3.2. Hence eq 3.7 gives

$$\dot{\bar{\gamma}} = \frac{1}{G}\int_0^{2\pi}(\sigma + \dot{\sigma} - \sin\gamma)\, P\, d\gamma \tag{3.8}$$

Note that this equation can be obtained directly from eq 3.4 if the average of both sides is taken.

Equations 3.6 and 3.8 are the basic set of equations in our model. For the stress-controlled case, eq 3.6 is solved for $P(\gamma,t)$ and then the macroscopic shear rate is calculated by eq 3.8, while for the strain-controlled case, eqs 3.6 and 3.8 must be solved simultaneously.

3.3. Stability Analysis. We shall now study the stability of the solutions to eq 3.6. Suppose that at time $t = 0$ the distributions of γ_i are sharply peaked around $\bar{\gamma}$. We then ask whether or not the distribution of γ will broaden with time for a given value of $\sigma(t)$ (stress-controlled case) or $\bar{\gamma}(t)$ (strain-controlled case).

To answer this question, we assume that the distribution function can be written as

$$P(\gamma,t) = (2\pi\alpha)^{-1/2}\exp\left[-\frac{1}{2\alpha(t)}[\gamma - \bar{\gamma}(t)]^2\right] \tag{3.9}$$

and study whether or not $\alpha(t)$ grows in time. Such a distribution function is reasonable when the system is characterized by very many layers and by small fluctuations in γ_i.

If $\alpha(t)$ is small, $P(\gamma,t)$ is sharply peaked around $\bar{\gamma}(t)$ and hence $\bar{\gamma}(t)$ satisfies the equation of motion without fluctuations

$$\dot{\bar{\gamma}} = \frac{\sigma + \dot{\sigma} - \sin(\bar{\gamma})}{G} \tag{3.10}$$

To obtain the time evolution of $\alpha(t)$, we multiply both sides of eq 3.6 by $(\gamma - \bar{\gamma}(t))^2$ and integrate over γ. After integration by parts, we obtain

$$\frac{d}{dt}\langle(\gamma - \bar{\gamma})^2\rangle = D\left\langle\frac{\partial^2}{\partial\gamma^2}(\gamma - \bar{\gamma})^2\right\rangle - 2\left\langle(\gamma - \bar{\gamma})\frac{\partial U}{\partial \gamma}\right\rangle \tag{3.11}$$

where $\langle ... \rangle = \int d\gamma ... P(\gamma,t)$. The last term on the right hand side of eq 3.11 can be evaluated by making a Taylor series expansion of $\partial U/\partial\gamma$ around $\bar{\gamma}$, *i.e.* $\partial U/\partial\gamma = \partial U/\partial\gamma|_{\bar{\gamma}} + (\gamma - \bar{\gamma})\partial^2 U/\partial\gamma^2|_{\bar{\gamma}}$. Substituting this into eq 3.11 and doing the integral,[17] we have

$$\frac{d\alpha}{dt} = 2D - \frac{2\cos\bar{\gamma}}{G}\alpha(t) \tag{3.12}$$

Thus we find that $\alpha(t)$ increases when $\cos\bar{\gamma}$ becomes negative.

The above analysis is essentially equivalent to the linear stability analysis outlined in section 2 and is limited to the regime of small $\alpha(t)$. When $\alpha(t)$ becomes large, various types of bifurcations take place. We shall discuss such behavior in the following section for the cases of steady shear flow, stress relaxation after a step-strain, and oscillatory shear strain.

4. Analysis of Rheological Flows

4.1. Steady Shear Flow. First we consider a steady shear flow. Such steady flow may be realized in either strain-controlled or stress-controlled experiments. In the present analysis, it is convenient to regard it as a stress-controlled experiment.

If fluctuations are not taken into account, the shear strain is easily obtained from eq 2.10. For $\sigma < 1$, γ approaches a constant value determined by $\sin\gamma = \sigma$. This corresponds to elastic deformation of the ordered phase. On the other hand if $\sigma > 1$, γ increases without bound, with $\dot{\gamma}(t)$ being a periodic function of t. This corresponds to the flow of the ordered phase. We shall now study such behavior in more detail using the diffusion equation approach.

From eq 3.6 it follows that the steady state distribution function $P_{st}(\gamma)$ satisfies

$$D\frac{\partial P_{st}}{\partial\gamma} + \frac{\partial U}{\partial\gamma}P_{st} = \text{constant} \tag{4.1}$$

Under the periodic boundary condition, eq 4.1 is solved as

$$P_{st}(\gamma) = C\exp[-U(\gamma)/D]\left[\int_\gamma^{2\pi} d\gamma' \exp[U(\gamma')/D] + \exp\left(-\frac{2\pi\sigma}{DG}\right)\int_0^\gamma d\gamma' \exp[U(\gamma')/D]\right] \tag{4.2}$$

where C is the normalization constant determined by eq 3.3. The resulting shear rate obtained from eq 3.8 is

$$\dot{\bar{\gamma}} = 2\pi DC\left[1 + \exp\left(-\frac{2\pi\sigma}{DG}\right)\right] \simeq \left[\frac{1}{2\pi D}\int_0^{2\pi} d\gamma \exp[-U(\gamma)/D]\int_\gamma^{2\pi} d\gamma' \exp[U(\gamma')/D]\right]^{-1} \tag{4.3}$$

where we have neglected the terms proportional to $\exp[-2\pi\sigma/DG]$, which are much less than unit for $D \ll 1$ (*i.e.* weak disorder).

The characteristic shapes of $U(\gamma)$ from eq 3.5 are shown in Figure 2 for $G = 10$ and values of σ larger and smaller than unity. If $\sigma < 1$, $U(\gamma)$ has a local maximum at γ_p and a local minimum at γ_v, corresponding to the positions of mechanical equilibrium, $\sigma = \sin\gamma$; γ_v corresponds to stable equilibrium and γ_p to unstable equilibrium. On the other hand, if $\sigma > 1$, $U(\gamma)$ decreases monotonically with the increase of γ.

For small values of D, the integral in eq 4.2 can be evaluated by expanding $U(\gamma)$ around its maximum value. As an example, we evaluate the integral $\int_\gamma^{2\pi} d\gamma' \exp[U(\gamma')/D]$ for the case of $\sigma < 1$. If $\gamma < \gamma_p$, the maximum of the integrand is located at γ_p, while it is at γ if $\gamma > \gamma_p$. In each

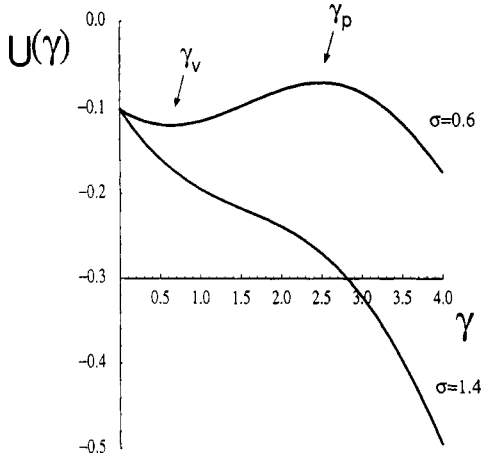

Figure 2. Plots of $U(\gamma)$ vs γ for $\sigma = 0.6$ and $\sigma = 1.4$. The curve for $\sigma = 0.6$ has a local minimum at γ_v and a local maximum at γ'_p corresponding to positions of stable and unstable mechanical equilibrium, while the curve for $\sigma = 1.4$ is monotonically decreasing, implying shear flow of the mesophase.

case, we evaluate the integral using the following approximation:

$$U(\gamma') = U(\gamma_p) + \frac{1}{2}\frac{\partial^2 U}{\partial \gamma^2}(\gamma_p)(\gamma' - \gamma_p)^2 \qquad \gamma < \gamma_p$$

$$U(\gamma') = U(\gamma) + \frac{\partial U}{\partial \gamma}(\gamma)(\gamma' - \gamma) \qquad \gamma > \gamma_p \tag{4.4}$$

As a result we have

$$\int_\gamma^{2\pi} d\gamma' \exp[U(\gamma')/D] = \begin{cases} |2\pi D/U''(\gamma_p)|^{1/2} \exp[U(\gamma_p)/D] & \gamma < \gamma_p \\ -(D/U'(\gamma)) \exp[U(\gamma)/D] & \gamma > \gamma_p \end{cases} \tag{4.5}$$

Where $U'(\gamma) \equiv \partial U/\partial\gamma$ and $U''(\gamma) \equiv \partial^2 U/\partial\gamma^2$. Thus, we obtain the following results.

(A) $\sigma < 1$ (Elastic Regime). In this case, $P_{st}(\gamma)$ is sharply peaked at γ_v, and $\dot{\bar{\gamma}}$ is very small.

$$P_{st}(\gamma) = \begin{cases} \frac{1}{2\pi}|U''(\gamma_p)U''(\gamma_v)/U'(\gamma)^2|^{1/2} \exp[-\Delta U/D] & \gamma < \gamma_p \\ \frac{1}{\sqrt{2\pi}}|U''(\gamma_v)/D|^{1/2} \exp[-(U(\gamma) - U(\gamma_v))/D] & \gamma > \gamma_p \end{cases} \tag{4.6}$$

and

$$\dot{\bar{\gamma}} = |U''(\gamma_p)U''(\gamma_v)|^{1/2} \exp\left[-\frac{\Delta U}{D}\right] \tag{4.7}$$

where $\Delta U = U(\gamma_p) - U(\gamma_v) = [2(1-\sigma^2)^{1/2} + \sigma(\gamma_p - \gamma_v)]/G$ is the "activation energy" for flow. If σ is close to 1, $\Delta U \simeq (2(1-\sigma))^{3/2}/G$, and

$$\dot{\bar{\gamma}} \sim \exp\left[-\frac{[2(1-\sigma)]^{3/2}}{DG}\right] \tag{4.8}$$

(B) $\sigma > 1$ (Flow Regime). In this case, the system starts to flow, with $P_{st}(\gamma)$ and $\dot{\bar{\gamma}}$ given by

$$P_{st}(\gamma) = \frac{1}{2\pi\sqrt{\sigma^2 - 1}}[\sigma - \sin\gamma]^{-1} \tag{4.9}$$

and

$$\dot{\bar{\gamma}} = \frac{1}{G}\sqrt{\sigma^2 - 1} \tag{4.10}$$

Figure 3 shows $P_{st}(\gamma)$ for $\sigma = 0.6$, 1.0, and 1.4. Note the broadening of the peak for $\sigma \geq 1$. Figure 4 shows the

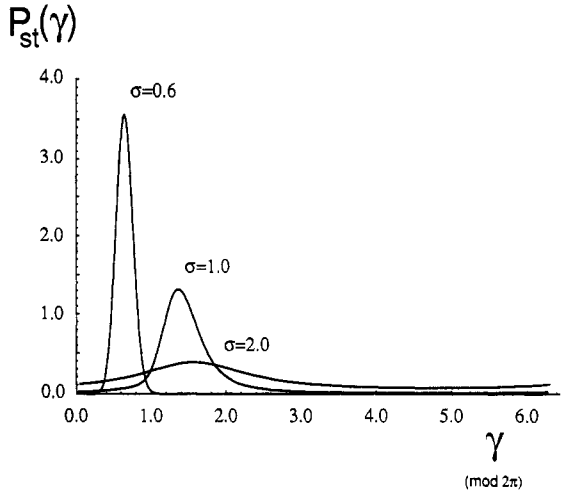

Figure 3. Plots of the steady state distribution function $P_{st}(\gamma)$ vs γ (mod 2π) for applied shear stresses $\sigma = 0.6$, $\sigma = 1.0$, and $\sigma = 2.0$ ($\sigma = 1.0$ is the critical shear stress for plastic flow). Note the significant broadening of $P_{st}(\gamma)$ for $\sigma = 2.0$. This corresponds to the viscous flow regime. These plots were obtained by numerical integration of eq 4.2 for $G = 10$ and $D = 10^{-3}$.

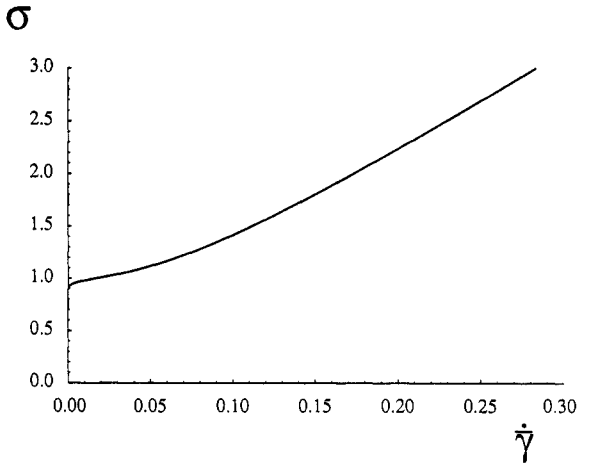

Figure 4. Plot of σ against $\dot{\bar{\gamma}}$ obtained from eq 4.3 for $G = 10$ and $D = 10^{-3}$. Note the yielding behavior at $\sigma \simeq 1$, the approach to linear viscous behavior ($\sigma \propto \dot{\bar{\gamma}}$) for $\sigma \gg 1$, and the intermediate region where $d^2\sigma/d\cdot\dot{\bar{\gamma}}^2 > 0$.

corresponding plot of σ against $\dot{\bar{\gamma}}$, showing the yielding behavior at $\sigma = 1$ and the approach to linear viscous behavior ($\sigma \propto \dot{\bar{\gamma}}$) for $\sigma \gg 1$. Here all calculations are made numerically using eqs 4.2 and 4.3 with $G = 10$ and $D = 10^{-3}$. We should mention one unusual feature of the steady flow behavior shown in Figure 4. In the conventional Bingham picture of viscoplastic flow, plots of σ against $\dot{\bar{\gamma}}$ are strictly convex, *i.e.* $d^2\sigma/d\dot{\bar{\gamma}}^2 \leq 0$. However, Figure 4 indicates a region at low σ for which $d^2\sigma/d\dot{\bar{\gamma}}^2 > 0$. Whether this is a general feature of mesoscopically ordered liquids or an artifact of our simple model is an issue for further study.

4.2. Stress Relaxation after Step-Strain. We now consider the stress relaxation experiment. Consider an external step-strain $\bar{\gamma}$ applied at time $t = 0$. If the applied strain $\bar{\gamma}$ is small, no slippage will take place. In such a case, the stress is calculated by eq 2.9;

$$\sigma(t) = \sin\bar{\gamma} + G\bar{\gamma}\exp(-t) \tag{4.11}$$

Thus, the stress relaxes to a finite value with a single relaxation time, $\tau = 1$. On the other hand, when $\bar{\gamma}$ becomes large, such a solution becomes unstable, and anomalous relaxation behavior occurs: a second relaxation event occurs at much later times.

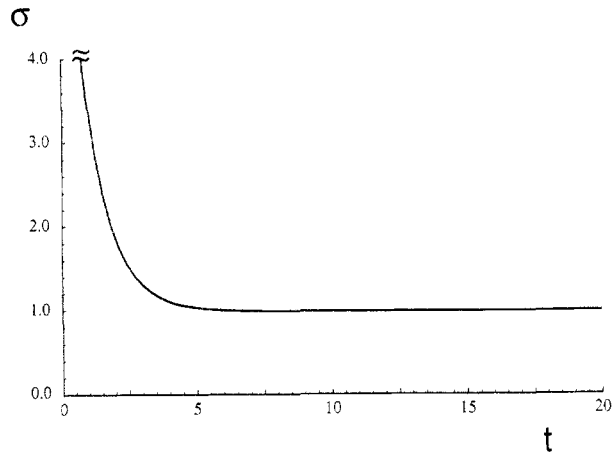

Figure 5. Plot of stress relaxation, $\sigma(t)$, vs t, after an applied step-shear strain of $\bar{\gamma} = 1.4$, indicating a single relaxation time $\tau \simeq 1$ associated with viscoelastic domain relaxation. This plot was obtained by numerical integration of eqs 2.8 and 2.10 for $G = 3$ and $\Delta\gamma = 0.15$.

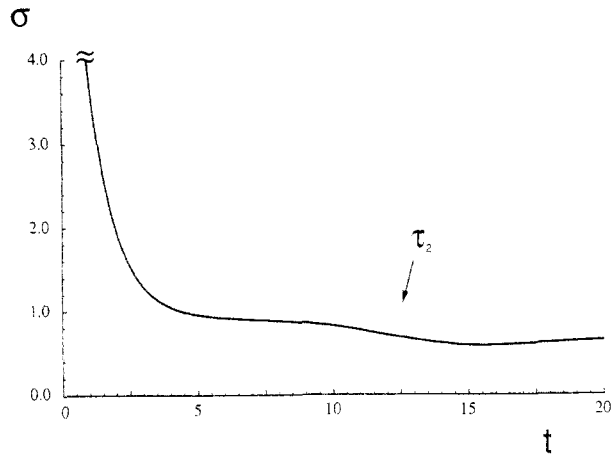

Figure 6. Plot of stress relaxation, $\sigma(t)$, vs t after an applied step-shear strain of $\bar{\gamma} = 2.0$, indicating a double stress relaxation process with relaxations times $\tau \simeq 1$ and $\tau_2 \simeq 12$, associated with viscoelastic domain relaxation and relative slippage of lattice planes, respectively. This plot was also obtained by numerical integration of eqs 2.8 and 2.10 for $G = 3$ and $\Delta\gamma = 0.15$.

The critical strain γ_c at which the instability takes place should be $\gamma_c = \pi/2$, the global stability limit that was identified in section 2 (the same results can be obtained easily by eq 3.12 as well). To study what happens for the $\bar{\gamma}$ above and below $\gamma_c = \pi/2$, we have made numerical calculations of the time evolution of eqs 2.8 and 2.10 subject to prescribed initial step-strains. We employed the standard fourth-order Runge–Kutta method[18] for integration of our equations of motion for γ_i. Initial conditions for γ_i were chosen randomly from the range $(\bar{\gamma} - \Delta\gamma, \bar{\gamma} + \Delta\gamma)$ subject to constraints imposed by eq 2.8 and for $\Delta\gamma/\bar{\gamma} \ll 1$. Calculations were made for a system of 10 lattice planes for several step-strains $\bar{\gamma}$ and various values of the parameters G and $\Delta\gamma$.

The results of numerical integration of eqs 2.8 and 2.10 for the case of $G = 3$ and $\Delta\gamma = 0.15$ are summarized in Figures 5–7. In Figure 5 we show a plot of σ against t for $\bar{\gamma} = 1.4$. This plot clearly shows a single relaxation time at $t \simeq \tau = 1$ associated with viscoelastic domain relaxation. In Figure 6 we show a plot of σ against t for $\bar{\gamma} = 2.0$, while in Figure 7 we show the corresponding plot of $\gamma_i(t)$ vs t for $i = 1 \ldots 10$. Figure 6 indicates that in addition to a rapid relaxation at $t = \tau$ associated with linear viscoelasticity, a second relaxation occurs at $t = \tau_2 \simeq 12$. In Figure 7, the trajectories of $\gamma_i(t)$ bifurcate at $t = \tau_2$ into groups with

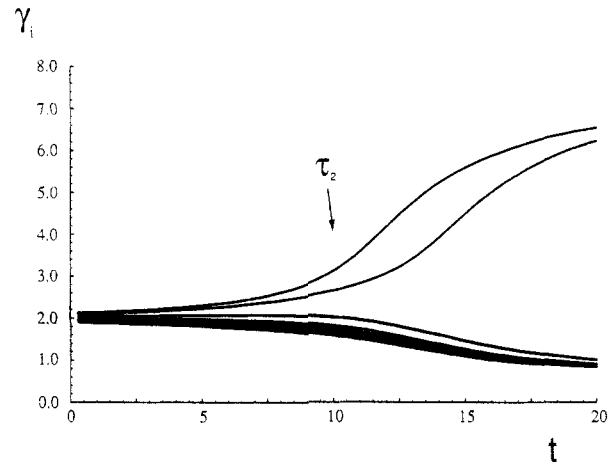

Figure 7. Plot of lattice plane shear strains γ_i vs t corresponding to the stress relaxation plot shown in Figure 6. This plot shows relative slippage of lattice planes occurring at $t \simeq \tau_2$. In this case, slippage occurs between layers 6 and 7, layers 7 and 8, layers 8 and 9, and layers 9 and 10, resulting in layers 7 and 9 advancing, and layers 1–6 and 10 retracting.

either $\gamma_i(t) > \bar{\gamma}$ or $\gamma_i(t) < \bar{\gamma}$, indicating the relative slippage of macrolattice planes. Figures 6 and 7 demonstrate unambiguously that the second stress relaxation time is associated with interlayer slippage. This behavior is in qualitative agreement with the numerical simulations reported in the previous paper.[1]

In order to demonstrate theoretically that the slippage of lattice planes can cause the anomalous slow second relaxation, we consider the case of a single slip plane,[19] in which case there are two groups of layers, an advancing group (with $\dot{\gamma}_i > 0$) and a retracting group (with $\dot{\gamma}_i < 0$). Then, the distribution function introduced in section 3 can be written as

$$P(\gamma,t) = \phi_a\delta(\gamma - \gamma_a(t)) + \phi_r\delta(\gamma - \gamma_r(t)) \qquad (4.12)$$

where ϕ_a and ϕ_r are constants independent of time. The values of ϕ_a and ϕ_r are determined at the initial stage of bifurcation and depend sensitively on the initial conditions. On the other hand, γ_a and γ_r are functions of time which we shall now determine. Let γ be defined by $\gamma(t) = \gamma_a(t) - \gamma_r(t)$. Using $\bar{\gamma} = \phi_a\gamma_a + \phi_r\gamma_r$, we can express γ_a and γ_r in terms of γ and $\bar{\gamma}$:

$$\gamma_a(t) = \bar{\gamma} + \phi_r\gamma(t)$$

$$\gamma_r(t) = \bar{\gamma} - \phi_a\gamma(t) \qquad (4.13)$$

The time evolution equation for $\gamma(t)$ is then obtained from

$$G\dot{\gamma}_a + \sin\gamma_a = G\dot{\gamma}_r + \sin\gamma_r = \sigma + \dot{\sigma} \qquad (4.14)$$

from which we find

$$\dot{\gamma} = \frac{1}{G}(\sin\gamma_a - \sin\gamma_r) = -\frac{2}{G}\cos\left(\bar{\gamma} - \frac{1}{2}(\phi_a - \phi_r)\gamma\right)\sin\left(\frac{\gamma}{2}\right) \qquad (4.15)$$

The right hand side is positive for $0 < \gamma < 2\pi$, so γ increases toward the stationary value 2π as time increases. Consequently, σ approaches $\sigma_\infty = \sin(\bar{\gamma} - 2\pi\phi_a)$. The characteristic time at which the slippage takes place can be estimated from the time required for γ to advance by π:

$$t_{slip} = \int_0^{\pi} \frac{d\gamma}{\dot{\gamma}} = -\frac{G}{2}\int_0^{\pi} \frac{d\gamma}{\sin(\gamma/2)\cos\left(\bar{\gamma} - \frac{1}{2}(\phi_a - \phi_r)\gamma\right)} \quad (4.16)$$

This integral diverges at $\gamma = 0$, so we replace the lower limit of the integral by a small value $\delta\gamma \ll 1$ to obtain

$$t_{slip} = \frac{G}{\cos\bar{\gamma}} \log\left(\frac{1}{\delta\gamma}\right) \quad (4.17)$$

Physically, $\delta\gamma$ is a measure of the level of disorder of the domains in the macrolattice. Intuitively, we would expect that almost perfectly ordered systems (very small $\delta\gamma$) should relax by slippage very slowly and that for a fixed level of disorder, t_{slip} should increase as $\bar{\gamma}$ approaches $\pi/2$ from above, reflecting the enhancement of metastability near $\gamma_c = \pi/2$. Also, samples with higher linear viscoelastic modulus G should have longer structural relaxation times. All of these expectations are satisfied qualitatively by eq 4.17. We may also make a quantitative comparison between eq 4.17 and the numerical results shown in Figure 6, for which $G = 3$, $\Delta\gamma = 0.15$, and $\tau_2 \simeq 12$. Taking $\delta\gamma = \Delta\gamma$ in eq 4.17, we find $t_{slip} = 13.7$, which is quite close to τ_2.

Although the phenomenological model presented here qualitatively reproduces the characteristic features of the simulation,[1] quantitative comparison is not possible since the parameters necessary to evaluate eq 4.17 are not all available. In our numerical calculations we have used rather disordered initial conditions ($\Delta\gamma/\bar{\gamma} = 0.075$) and step-strains that are not very close to γ_c, in order to minimize computation time. Hence, the resulting structural relaxation time $\tau_2 \simeq 12$ is not very large compared with the viscoelastic relaxation time $\tau = 1$. By decreasing the noise level or choosing a step-strain near the critical value, we can easily increase τ_2 computed numerically by a factor of 5 to 10. In the simulations, however, the structural relaxation time of a well-ordered mesophase is very long: $\tau_2/\tau \simeq 10^2$ for a relatively large true shear strain of 0.4 ($\bar{\gamma} \simeq 2$ in our language; *cf.* eq 2.2). Our simple model may therefore be too crude to make quantitative predictions of this sort.

4.3. Oscillatory Shear. We shall now consider the oscillatory shear response when the shear strain is driven sinusoidally as

$$\bar{\gamma}(t) = A \sin \omega t \quad (4.18)$$

First we study the stability of the homogeneous structure. In this case, eq 3.12 becomes

$$\frac{d\alpha}{dt} = 2D - 2\frac{\cos(A \sin \omega t)}{G}\alpha \quad (4.19)$$

This equation is easily solved by using

$$F(t) = \frac{2}{G}\int_0^t dt' \,[\cos(A \sin \omega t')] \quad (4.20)$$

to obtain

$$\alpha(t) = \alpha_0 \exp[-F(t)] + 2D\int_0^t dt' \exp[-[F(t) - F(t')]] \quad (4.21)$$

The integrand of eq 4.20 is a periodic function of t with periodicity $T = 2\pi/\omega$. If $F(T) < 0$, the amplitude of $\alpha(t)$ increases after one period of oscillation, implying that $\alpha(t)$ diverges with increasing t; *i.e.* the homogeneous solution becomes unstable. The critical amplitude A_c at which this instability occurs is obtained from $F(T) = 0$. This criterion gives a critical amplitude A_{c_1} given by $J_0(A_{c_1}) = 0$ where $J_0(x)$ is the Bessel function of order 0. Thus, we find

$$A_{c_1} = 2.405 \quad (4.22)$$

If $F(T) > 0$, $\alpha(t)$ asymptotically decreases to zero with increasing t. Notice, however, that the above linear stability analysis is valid provided that $\alpha(t)$ is small for all t. But, according to eq 4.19, $d\alpha(t)/dt$ is positibe during some portion of an oscillation period. If the duration of positive $d\alpha(t)/dt$ is sufficiently long, which is the case for small ω, then $\alpha(t)$ can become quite large and can be outside the linear regime. Such an unstable mode occurs at low frequencies only for negative $\cos\bar{\gamma}(t)$, *i.e.* for an amplitude that is larger than $\pi/2$. Therefore, the second critical amplitude is

$$A_{c_2} = \pi/2 \simeq 1.56 \quad (4.23)$$

Thus, the homogeneous solution is globally stable for $A < A_{c_2}$, and linearly unstable for $A > A_{c_1}$. For amplitudes lying between these values, $A_{c_2} < A < A_{c_1}$, the stability of the homogeneous solution is conditional,[20] and the critical amplitude is expected to be frequency dependent. Nonlinear stability analysis is necessary to ascertain this frequency dependence. However, we expect that as $\omega \to \infty$, the homogeneous solution becomes unstable only at the linear stability point, A_{c_1}; while for $\omega \to 0$, it becomes unstable at A_{c_2}.

In order to ascertain the frequency dependence of the stability limits and the resulting stress–strain patterns in the slipping and nonslipping regimes, we have made numerical calculations of the time evolution of eqs 2.8 and 2.10 under imposed periodic shear strains. As in the step-strain case, we employed the Runge–Kutta method for computing the time evolution of our equations of motion for $\gamma_i(t)$ and $\sigma(t)$. Initial conditions for γ_i were chosen randomly from the range $(-\Delta\gamma, \Delta\gamma)$ subject to the constraint imposed by eq 2.8 that $\bar{\gamma}(0) = 0$ and for $\Delta\gamma/A \ll 1$. In addition, small random fluctuations in the range $(-\Delta\gamma, \Delta\gamma)$ were added to randomly chosen γ_i at every time step subject to eq 2.8, to account for the noise term introduced in section 3. Calculations were made for a system of 10 lattice planes for various amplitudes and frequencies, A and ω, and values of the parameters G and $\Delta\gamma$. The results of numerical integration of eqs 2.8 and 2.10 are summarized in Figure 8, while specific examples of stress–strain patterns for $G = 2$ and $\Delta\gamma = 10^{-3}$ at low and high ω and for large and small A are shown in Figure 9. In the following, we discuss separately the behavior for low and high frequencies.

In the limit of $\omega \to 0$, the solution is quasistationary, and the transition to a slipping solution occurs at the global stability point, $A = A_{c_2} = \pi/2$, as expected. For $A < \pi/2$, the homogeneous solution is stable, and the constitutive relation is essentially that of an elastic material:

$$\sigma = \sin\bar{\gamma} \quad (4.24)$$

Accordingly, the Lissajous pattern has the form of a strain-softened pattern; *i.e.* the stress decreases with increasing strain near the extremum of the stress–strain curve. Figure 9a shows such a pattern obtained for $\omega = 10^{-2}$ and $A = 1.4$.

However, for $A > \pi/2$, the homogeneous solution bifurcates to a slipping solution, and the Lissajous pattern adopts a lozenge shape like that shown in Figure 9b for $\omega = 10^{-2}$ and $A = 3.0$. This unusual stress–strain pattern can be understood as follows. Consider the idealized sketch of such a low frequency lozenge pattern given in Figure

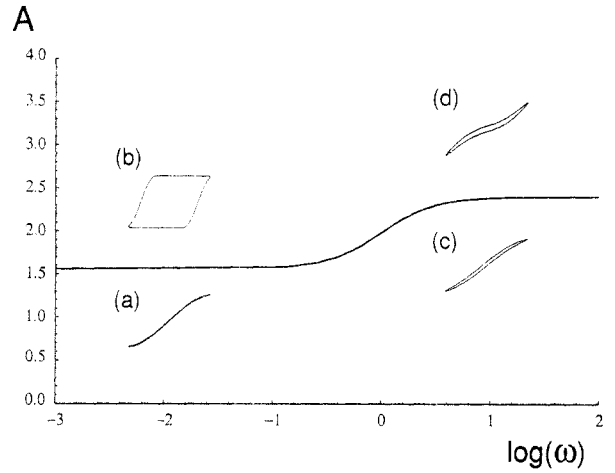

Figure 8. Sketch of the various regimes of oscillatory stress–strain patterns for $G = 2$ and $\Delta\gamma = 10^{-3}$ as a function of frequency ω and shear strain amplitude A. The curve divides the diagram into a region of ordinary elastic and viscoelastic behavior at low shear strain amplitude and a region of anomalous nonlinear behavior associated with lattice plane slippage at high shear strain amplitude. The critical amplitude separating these regimes is $A = A_{c_2} = \pi/2$ at low frequencies, and $A = A_{c_1} \simeq 2.4$ at higher frequencies, as discussed in the text. The Lissajous patterns (a)–(d) are sketches of typical stress–strain patterns obtained at low and high ω and large and small A.

10. Initially, all layers start with approximately zero displacement, $\gamma_i(0) \simeq 0$, and follow the homogeneous solution. Accordingly, the stress $\sigma(t)$ initially increases following eq 4.24 (*cf.* the interior line in Figure 10). However, as $\bar{\gamma}$ approaches $\pi/2$, the homogeneous solution becomes unstable (see eq 3.12) and slip planes develop. Thus for $\bar{\gamma} > \pi/2$, further macroscopic strain is accomplished by slippage (with steady shear rate $\dot{\bar{\gamma}} \simeq A\omega$) up to $\bar{\gamma} = A$. During this period, most layers have their local strain frozen around $\gamma_i = \pi/2$, resulting in a constant stress level $\sigma = 1$ from the initiation of slippage at $\bar{\gamma} \simeq \pi/2$ up to $\bar{\gamma} = A$ (*cf.* the top edge of Figure 10). The precise value of $\bar{\gamma}$ at which slipping begins depends critically on the level of disorder in the system; roughly speaking, slippage occurs as soon as at least one layer accumulates $\pi/2$ of shear strain. Since the system is slightly disordered, with a distribution of γ_i which is peaked at $\bar{\gamma}$ (*cf.* the $\sigma = 1$ curve in Figure 3), this slippage generally begins before $\bar{\gamma} - \pi/2$. When $\bar{\gamma} = A$, the applied strain rate changes sign, and the layers once again follow the homogeneous solution until $\bar{\gamma}$ decreases by roughly π (*cf.* the right edge of Figure 10). At this point, $\bar{\gamma} \simeq A - \pi$ and slip planes develop once again. Subsequent macroscopic strain up to $\bar{\gamma} = -A$ occurs through slippage with $\sigma = -1$ (*cf.* the bottom edge of Figure 10). Analogous processes produce the left and top edges of Figure 10, thus completing one cycle of deformation. The steady state pattern is therefore a lozenge-shaped pattern as shown in Figure 9b. However, as the level of disorder in the numerically produced patterns is substantial, the range of $\bar{\gamma}$ for which the layers follow the homogeneous, nonslipping solution is somewhat less than $\Delta\bar{\gamma} = \pi$, as can be seen by examining the left and right edges of the pattern in Figure 9b. We note that such lozenge patterns were also observed in the computer simulations reported in the previous paper[1] for relatively large amplitude, low frequency applied shear strains.

In the limit of high frequency, $\omega \to \infty$, homogeneous and slipping solutions analogous to those found in the low frequency case exist, as shown in Figure 9c,d, respectively. However, numerical results indicate that, as anticipated, the linear stability limit, A_{c_1}, is the boundary between homogeneous and slipping solutions (see Figure 8). If $A < A_{c_1}$, the homogeneous solution is stable, so that the shear stress is obtained from eq 2.9 evaluated at $\gamma_i(t) = \bar{\gamma}$ in the limit $\omega \to \infty$ as

$$\sigma = \sin\bar{\gamma} + G\bar{\gamma} \tag{4.25}$$

Thus the Lissajous is that of strain-softening; *i.e.* stress decreases with increasing strain near the extremum of the stress–strain curve (Figure 9c; $\omega = 5$, $A = 2.0$).

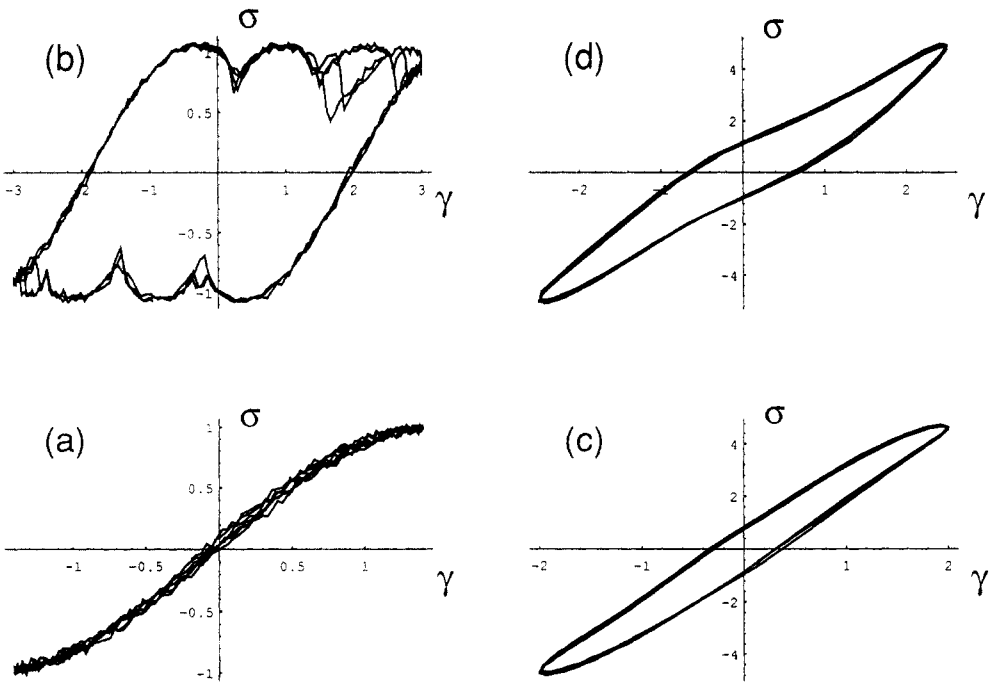

Figure 9. Examples of the Lissajous patterns obtained at low and high ω and large and small A through numerical integration of eqs 2.8 and 2.10 with $G = 2$ and $\Delta\gamma = 10^{-3}$ and for 10 lattice planes. The stress–strain patterns are labeled (a)–(d) in accordance with those sketched in Figure 8. Patterns a and b are low frequency patterns with $\omega = 10^{-2}$, corresponding to $A = 1.4$ and $A = 3.0$, respectively, while patterns c and d are high frequency patterns with $\omega = 5$, corresponding to $A = 2.0$ and $A = 2.5$, respectively. Large fluctuations in the low frequency patterns are primarily due to the small system size.

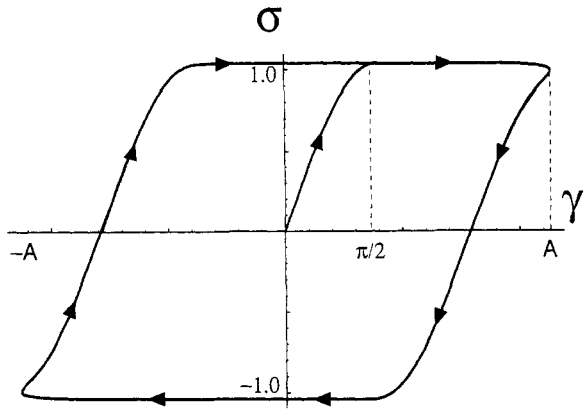

Figure 10. Sketch of the lozenge stress–strain pattern obtained for low frequency, large amplitude shear strains, indicating the transient behavior at $t = 0_+$ and the resulting steady state cycle.

If $A > A_{c_1}$, an instability takes place. The numerical calculations indicate that in such a state, the layers separate into two groups: one oscillating around $\gamma = \pi$, and another oscillating around $\gamma = -\pi$; *i.e.* half the layers follow $\gamma_a(t) = \bar{\gamma} + \pi$, and the rest follow $\gamma_r(t) = \bar{\gamma} - \pi$. Notice that such a solution is compatible with eqs 2.7 and 2.8. Thus, the stress in this case is given by eq 2.9 with $\gamma_i(t) = \bar{\gamma} \pm \pi$ and $\omega \to \infty$:

$$\sigma = -\sin \bar{\gamma} + G\bar{\gamma} \tag{4.26}$$

where we have used $\sin(x \pm \pi) \equiv -\sin x$. Notice that in this case, the Lissajous pattern is that of strain-hardening; *i.e.* the stress increases with increasing strain near the extremum of the stress–strain curve (Figure 9d; $\omega = 5$, $A = 2.5$).

5. Discussion

We have presented a statistical theory for the rheology of block copolymer liquids forming a macrolattice. Our theory is based on a multilayer model for the microphase-separated state and phenomenological interlayer stress–strain relations that account for the equilibrium periodicity of the mesophase, as well as the viscoelastic features of domain relaxation. This approach is valid for time scales much longer than those characterizing chain relaxation processes in mesophases and hence is complimentary to existing theories of mesophase rheology which focus on relaxation of interdomain entanglements and local collective modes of domain relaxation.[7,8] The outstanding feature of our theory is the prediction of nonlinear rheological behavior due to the relative slippage of layers in response to sufficiently large applied strains. In particular, our theory predicts (i) viscoplastic flow behavior with a true yield stress (*cf.* Figure 4), (ii) a novel double stress relaxation in response to sufficiently large applied step-strains that is due to a relatively slow structural relaxation process associated with interlayer slippage (*cf.* Figures 6 and 7), and (iii) unusual nonlinear stress–strain patterns in response to applied oscillatory shear strains of sufficient amplitude, including lozenge shaped stress–strain patterns at very low frequencies and strain-hardened-type patterns at higher frequencies (*cf.* Figure 9b,d). These patterns were shown to result from periodic transitions from homogeneous to slipping-layer deformations, and stability limits at small and large frequencies were identified, resulting in a mode diagram of homogeneous vs slipping behavior as a function of the amplitude and frequency of applied shear strain (*cf.* Figure 8).

The slipping behavior exhibited by ordered copolymer mesophases apparently differs qualitatively from the usual mechanism for plastic deformation in metals.[21] In metals, plastic flow occurs through the creation of topological defects (*e.g.* disclinations and dislocations) and their motion along crystallographic planes. However, in ordered liquids, such as copolymer mesophases, topological defects are not necessary for plastic behavior; slight positional disorder in the macrolattice or polydispersity in domain size seems to be sufficient to allow slippage along crystallographic planes. Furthermore, in these liquidlike systems, large shear strains are completely reversible. This is certainly not the case for metals, for which material properties are strain-history dependent and for which strains of more than a few percent often result in fracture. Macromolecular mesophases are very soft in the molten state; their cohesive energies are low in comparison with ordinary solids and they are very easily deformed. This softness is the key feature which distinguishes the nonlinear rheological properties of these materials from the viscoplastic behavior of ordinary deformable solids.

The above results for applied step and oscillatory strains [(ii) and (iii)] are in qualitative agreement with the simulation results presented in the previous paper.[1] In the case of applied oscillatory shears of low frequency ($\omega = 10^{-4}$),[22] the simulations indicated a transition from elastic stress–strain patterns to nonlinear lozenge patterns as the amplitude of the applied shear was increased from $\Gamma = 0.2$ to $\Gamma = 0.4$ (compare Figure 5 of ref 1 with Figure 9a,b). Furthermore, for the case of applied oscillatory shear strains of moderate amplitude ($\Gamma = 0.4$), the simulations indicated a transition from the usual viscoelastic stress–strain patterns to the nonlinear lozenge patterns as ω was decreased from $\omega = 10^{-3}$ to $\omega = 10^{-4}$. This is consistent with our results for the case of strain amplitudes which are intermediate to the low and high frequency stability bounds identified in section 4.3, $A_{c_2} < A < A_{c_1}$. This amplitude range corresponds to true shear strain amplitudes of $0.29 < \Gamma < 0.44$ in the simulations (*cf.* eq 2.2). In this case, by lowering the frequency at fixed strain amplitude $\Gamma = 0.4$, the transition from a viscoelastic pattern like that in Figure 9c to a lozenge pattern like that in Figure 9b is indeed possible (*cf.* Figure 8). Finally, we note that the double stress relaxation behavior after an applied step-strain obtained in section 4.2 qualitatively reproduces the step-strain result of the simulations (Compare Figures 8 and 9 of ref 1 with Figures 5 and 6 above). Quantitative comparison is not possible at this stage since the material parameters necessary for comparison are unknown.

The theory we have presented may be relevant to existing experimental results on microphase-separated block copolymer solutions in selective solvents. Detailed studies have been made of the rheology and equilibrium structure of microphase-separated solutions of styrene–butadiene block copolymers in selective solvents.[11-13] Such mesophases typically consist of cores of precipitated blocks of one species surrounded by dissolved cilia of the second species. For the block ratios primarily studied, simple cubic lattices are formed in the microphase-separated state. Both the rheology and equilibrium structure, as determined by small angle X-ray scattering (SAXS), were studied as a function of temperature and copolymer concentration. The equilibrium and rheological properties of these materials were found to be strongly correlated as follows. Above a critical concentration and below a critical temperature, these mesophases exhibited strong nonlinear rheological behavior. Viscoplastic flow behavior with a true yield stress was observed (*cf.* Figures 1 and 6 of ref 11). Nonlinear response to applied oscillatory shear strain

was also observed, including lozenge-shaped Lissajous patterns for relatively large amplitude, low frequency strains similar to those shown in section 4.3 (*cf.* the top portions of Figures 10 and 14 of ref 13). In these experimental studies, a transition from elastic to nonlinear response with increasing strain amplitude was observed, and for the case of relatively large amplitude shear strains, an *increase* in the nonlinearity of the response with *decreasing* frequency was also reported, in qualitative agreement both with the results reported in this work and with the simulations reported in the previous paper. We should note that the critical strain amplitude in these experiments (a true shear strain of less than $\gamma = 0.10$) was much smaller than that found in the present work or in the simulations. However, the mesophases studied in the experiments are much different in nature than the cylindrical mesophases of molten block copolymer in our work. The cores of the microphase-separated copolymer solutions studied were quite dense spheres of the immiscible species in an entangled solution of the dissolved cilia of the second species. Such an arrangement is like a colloidal crystal, and is expected to be more sensitive to applied shears than a molten copolymer mesophase in the weak segregation regime.

Significantly, the critical concentration and temperature for nonlinear rheological behavior in the experiments coincided with the macrolattice order–disorder transition determined by SAXS measurements. In particular, the critical temperature corresponded to the temperature at which *long-range* order disappeared, leading Watanabe *et al.* to conclude that long-range order of the macrolattice is a necessary condition for the unusual nonlinear rheological behavior observed.[11] Thus, one would expect that the mechanism for this nonlinear behavior in concentrated block copolymer solution mesophases is the relative slippage of macrolattice planes, as we have argued for microphase-separated block copolymer melts.

However, we note that the situation for imperfectly ordered mesophases may be quite different. In this case, the role of topological defects in the rheology may be significant.[6] In practice, polycrystalline samples may be perfectly ordered and their defects removed by the application of an extended period of oscillatory shear strain.[6]

We expect that the nonlinear rheological behavior associated with slippage is a common feature of many ordered liquids, including charged colloidal suspensions[23] ordered microemulsions,[24] and regular foams.[25] Indeed, charged latex systems have been reported to exhibit Bingham plasticity and iridescent color indicative of long-range colloidal crystalline order.[26] Watanabe *et al.* also investigated the rheological response of aqueous charged latex suspensions to oscillatory shear strain.[11] They found nonlinear behavior at high latex concentrations that is qualitatively similar to their microphase-separated block copolymer solution results, including the novel lozenge-shaped Lissajous pattern at low frequencies (*cf.* Figure 5a of ref 11). Recently, Vollmer *et al.*[24] have produced ordered, monodisperse microemulsions of water/AOT/isooctane by adding small amounts of oxyethylene/isoprene/oxyethylene triblock copolymer. Such a system may also have such unusual nonlinear rheological behavior.

We have presented a simplified phenomenological theory in this paper, which however exhibits rich and interesting rheological behavior. It would be interesting to extend this work to realistic models of ordered copolymer mesophases. For instance, comparison of the rheological behavior of block copolymer melts in the strong and weak segregation regimes could be made within the present theoretical framework. Another interesting extension would be the study of added homopolymer or triblock copolymer on the rheological behavior of diblock copolymer mesophases. Indeed, interesting experimental studies of the effects of added homopolymer and triblock copolymer on the rheology of microphase-separated diblock copolymer solutions have already been made.[13] Finally, a more technical extension of the theory would be a more detailed study of the conditional stability of the intermediate frequency rheological response within the present simplified theoretical model. This would involve nonlinear stability analysis of a coupled multilayer viscoelastic system.

Acknowledgment. We are grateful to Dr. K. Sekimoto and Dr. H. Watanabe for interesting and informative discussions. This work was supported in part by the Grant-in-Aid for Scientific Research administered by the Ministry of Education, Science, and Culture of Japan and by the Tokuyama Science Foundation. J.L.H. was supported by a postdoctoral fellowship from the Japan Society for the Promotion of Science.

References and Notes

(1) Ohta, T.; Enomoto, Y.; Harden, J. L.; Doi, M. Preceding paper in this issue.
(2) Bates, F. S. *Macromolecules* **1984**, *17*, 2607.
(3) Fredrickson, G. H.; Larson, R. *J. Chem. Phys.* **1987**, *86*, 1553.
(4) Rosedale, J. H.; Bates, F. S. *Macromolecules* **1990**, *23*, 2329.
(5) Koppi, K. A.; Tirrell, M.; Bates, F. S.; Almdal, K.; Colby, R. H. *J. Phys. Fr. II* **1992**, *2*, 1941.
(6) Larson, R. G.; Winey, K. I.; Patel, S. S.; Watanabe, H.; Bruinsma, R. *Rheol. Acta*, submitted for publication (and references cited therein).
(7) Witten, T. A.; Leibler, L.; Pincus, P. *Macromolecules* **1990**, *23*, 824.
(8) Rubinstein, M.; Obukhov, S. P. *Macromolecules*, in press.
(9) Joanny, J.-F. *Langmuir* **1992**, *8*, 989.
(10) Kawasaki, K.; Onuki, A. *Phys. Rev. A* **1990**, *42*, 3664.
(11) Watanabe, H.; Kotaka, T.; Hashimoto, T.; Shibayama, M.; Kawai, H. *J. Rheol.* **1982**, *26*, 153.
(12) Hashimoto, T.; Shibayama, M.; Kawai, H.; Watanabe, H.; Kotaka, T. *Macromolecules* **1983**, *16*, 361.
(13) Watanabe, H.; Kotaka, T. In *Current Topics in Polymer Science*; Ottenbrite, R. M., Utracki, L. A., Inoue, S., Eds.; Hanser Publishers: New York, 1987; Vol. II, pp 61–96 (a review of experimental results).
(14) Watanabe, H.; Kotaka, T. *Macromolecules* **1983**, *16*, 1783.
(15) Helfand, E.; Wasserman, Z. R. *Macromolecules* **1980**, *13*, 994. Helfand, E.; Wasserman, Z. R. In *Developments in Block Copolymers-1*; Goodman, I., Ed.; Applied Science: New York, 1982 (see also references therein).
(16) Van Kampen, N. G. *Stocastic Processes in Physics and Chemistry*; North Holland: Amsterdam, 1981.
(17) Since $\alpha(t)$ is assumed to be very small in eq 3.9, we may extend the domain of integration here and in eq 3.3 to $-\infty < \gamma < \infty$.
(18) Press, W. H.; Flannery, B. P.; Teukolsky, S. A.; Vetterling, W. T. *Numerical Recipes: The Art of Scientific Computing*; Cambridge University Press: Cambridge, U.K., 1986.
(19) Note that multiple slip planes generally occur simultaneously. In the numerical calculation depicted in Figure 7, for instance, slip planes developed between layers 6 and 7, layers 7 and 8, layers 8 and 9, and layers 9 and 10. In principle, there should be different advancing and retracting groups corresponding to each slip plane.
(20) Manneville, P. *Dissipative Structures and Weak Turbulence*; Academic Press: New York, 1990.
(21) Haasen, P. *Physical Metallurgy*; Cambridge University Press: Cambridge, U.K., 1978.
(22) Note that $\omega = 10^{-4}$ in the units of ref 1 corresponds to approximately $\omega = 10^{-2}$ in our units; the characteristic time in ref 1 is the chain relaxation time, while here it is the domain relaxation time.
(23) Russel, W. B.; Saville, D. A.; Schowalter, W. R. *Colloidal Dispersions*; Cambridge University Press: Cambridge, U.K., 1989.
(24) Volmer, D.; Hofmeier, U.; Eicke, H.-F. *J. Phys. Fr. II* **1992**, *2*, 1677.
(25) Kraynik, A. M. *Annu. Rev. Fluid Mech.* **1988**, *20*, 325. Reinelt, D. A.; Kraynik, A. M. *J. Fluid Mech.* **1990**, *215*, 431.
(26) Mitaku, S.; Ohtsuki, T.; Okano, K. *J. Soc. Rheol. Jpn.* **1979**, *7*, 47.